J. Fluid Mech. (1996), *vol.* 314, *pp.* 299–314

Formation of cells in natural convection in a vertical slot at large Prandtl number

By SHUNICHI WAKITANI

Department of Mechanical Engineering, College of Industrial Technology,
1-27-1 Nishikoya, Amagasaki 661, Japan

(Received 21 December 1994 and in revised form 9 October 1995)

This paper presents several features at supercritical conditions of natural convection of large Prandtl number fluids in a vertical slot. Both experimental and numerical results show that even at slightly supercritical conditions the multicellular flow is in an unsteady state which is attributed to the moving and merging of cells. The effect of variable viscosity on the unsteadiness is investigated numerically. Successive merging and appearance of cells is characteristic of this convection so that the number of secondary cells changes with time. The bifurcation phenomena characterized by several modes of unsteady cellular flow are examined.

1. Introduction

Since the pioneering work of Batchelor (1954), the problem of natural convection in a vertical slot, or a tall cavity, with a constant temperature difference between the parallel sidewalls has continued to be studied analytically, experimentally and numerically by many investigators because of its importance in geophysical and engineering applications.

The independent parameters that describe the flow of a constant-viscosity fluid in a two-dimensional vertical slot are the Rayleigh number Ra, the Prandtl number Pr and the aspect ratio A, where

$$Ra = \frac{g\beta\Delta T W^3}{\nu\kappa}, \tag{1.1}$$

$$Pr = \nu/\kappa, \tag{1.2}$$

$$A = H/W, \tag{1.3}$$

with g the gravitational acceleration, β the thermal expansion coefficient, $\Delta T(= T_1 - T_2 > 0)$ the temperature difference between the sidewalls, W and H the width and height of the slot respectively, ν the kinematic viscosity, and κ the thermal diffusivity. It is well known that the flow can be classified into the conduction, the transition, and the boundary-layer regimes corresponding to small, intermediate, and high Rayleigh numbers, respectively (Eckert & Carlson 1961). Figure 1 shows the coordinate system used for the experimental and numerical work.

In a moderately tall cavity with a finite A, as Ra is increased the flow of fluids whose Pr is larger than about 50 enters the transition or boundary-layer regime with a vertical temperature stratification before the instability from the conduction regime occurs (Bergholz 1978; Lee & Korpela 1983). When Ra exceeds a first critical value Ra_c, the transition or boundary-layer regime of a large-Pr fluid becomes unstable and

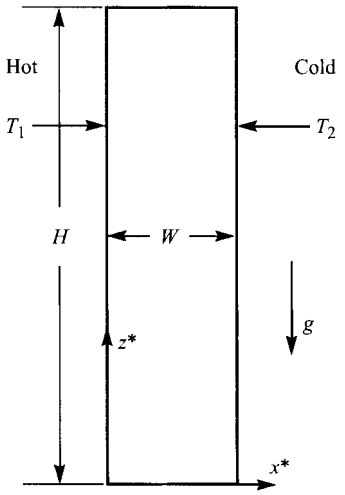

FIGURE 1. Vertical slot and coordinate system.

a unicellular convection breaks down into a multicellular convection arranged in a series of secondary cells. Then as Ra is increased up to about $2Ra_c$–$3Ra_c$, tertiary cells that are counter-rotating between the secondary cells are observed. The appearance of the secondary and tertiary cells in large-Pr fluids has been confirmed experimentally (Elder 1965; Seki, Fukusako & Inaba 1978; Chen & Thangam 1985; Wakitani 1994) and numerically (de Vahl Davis & Mallinson 1975).

Extensive time-dependent numerical calculations of multicellular convection were performed by Lee & Korpela (1983). They treated natural convection of a constant-viscosity fluid for Pr in the range 0–1000. Their computational result for $Pr = 0$ demonstrates that the number of secondary cells depends on the initial condition. However, it is unknown whether this result can be applied to large-Pr fluids. For $Pr = 1000$ and $A = 15$, without referring to the initial conditions, Lee & Korpela (1983) stated that the number of secondary cells at steady state changed from three to seven and then to five as Ra was increased. However, Chait & Korpela (1989) showed that for $Pr = 1000$, the secondary flow in a vertical slot with infinite A was periodic in time. We doubt whether the result of Lee & Korpela (1983) was in steady state.

As Ra is increased, numerical simulations with parameters appropriate to an air-filled vertical slot show a reverse transition from multicellular to unicellular structure (Roux *et al.* 1980; Lauriat & Desrayaud 1985; Le Quéré 1990). To our knowledge, there is no conclusive experimental evidence of the reverse transition. For $Pr = 0.71$ and $A = 16$, Le Quéré (1990) found the existence of several branches of solutions characterized by different numbers of cells. His unsteady calculation showed that the multicellular flow is substantially unsteady at some high Ra, and as Ra is gradually increased, the return to the unicellular pattern from the multicellular structure occurs through a gradual decrease in the number of cells. The multicellular convection was in the conduction regime in contrast to the case for large Pr and the unicellular solution was at steady state with a vertical temperature stratification. For large-Pr fluids, such a reverse transition has not been observed but a remaining secondary cell has been observed in the centre of the slot at high Ra (Wakitani 1994).

In this paper, we show experimentally the existence of continuous merging and appearance of secondary cells at the supercritical condition of natural convection of large-Pr fluids in a vertical slot. The merging and appearance are considered

characteristic for multicellular flow of large Pr in a vertical slot. Taking into account the temperature-dependent viscosity, we perform a two-dimensional numerical simulation for long enough in time to reach an asymptotic unsteady solution. The result demonstrates our experimental observations. The development of multicellular solutions is clarified numerically for a constant-viscosity fluid.

2. Experiments

2.1. *Experimental apparatus and method*

The same experimental apparatus and method were used in the present experiments as described in a previous paper (Wakitani 1994). A vertical slot was used of dimensions 300 mm in height (H) $\times$ 150 mm in depth $\times$ variable width (W, typically 15–30 mm). Silicone oils (Toshiba Silicone TSF451 series) with density $\rho = 935$ kg m^{-3}, $\nu = 10$ mm^2 s^{-1}, $\beta = 1.08 \times 10^{-3}$ K^{-1} ($Pr = 125$) and with $\rho = 968$ kg m^{-3}, $\nu = 100$ mm^2 s^{-1}, $\beta = 0.98 \times 10^{-3}$ K^{-1} ($Pr = 900$) at temperature 298 K were used as working fluids. They show about a 2% decrease in viscosity as temperature increases by 1 K. We evaluated physical properties of the fluids at the mean value, typically 298 $\pm$ 1 K, of the sidewall temperatures. The temperature differences ΔT were typically 9–40 K. The slot consists of two vertical sidewalls (340 mm $\times$ 190 mm) made of two copper plates 5 mm in thickness and a Pyrex glass frame of variable width 8 mm in thickness. Copper plates separate the slot from two water jackets, each with five separate water pipes. The flow rate in each pipe was controlled so that the sidewalls could be maintained at constant temperatures. The water jackets were insulated with styrofoam boards. The water temperatures in the jackets could be controlled by means of two constant-temperature baths (Neslab RTE-9 and EX-210).

To measure sidewall temperatures, nine sheathed copper–constantan thermocouples 1 mm in diameter were embedded in each copper plate through the water jacket. Seven of these thermocouples were located at intervals of 40 mm on the vertical centreline and others at the midheight of the slot. Fluid temperature was measured using a probe fabricated from a chromel–alumel thermocouple 50 μm in diameter. The probe was fed through a slit at the top of the slot. The measurements were performed at around half the depth. The thermocouple wires were connected to a digital data acquisition system (Scanner: Advantest R7210 and DVM: Advantest TR6851) controlled through a personal computer. With this system, voltage fluctuations could be measured to 0.1 μV.

A tracer injection method was used to visualize cellular patterns. Aluminium oxide powder mixed with the working fluid was carefully dropped into the fluid in the slot from the top of the slot. The aluminium oxide particles were illuminated by a laser light sheet from a 15 mW He–Ne laser through the top. The laser beam was expanded into a sheet in a plane at around half the depth using a cylindrical lens to obtain still photographs of cellular patterns. The photographs were taken with a long exposure of 15 s.

The width W of the slot varied by less than $\pm$0.1 mm over whole height. The maximum uncertainty associated with the length scale in the data reduction was $\pm$0.2 mm. The digital data acquisition system could detect temperature fluctuations of 0.0025 K (0.1 μV). Taking into account all of the errors induced by thermocouples, reference junction compensation, temperature difference among terminals, e.m.f. at scanner junction, DVM accuracy and output offset, the entire accuracy of the temperature measurements was within $\pm$0.1 K. The uncertainty associated with the physical properties of silicone oils in the data reduction was less than $\pm$1%.

First, two constant-temperature baths are heated. After the temperatures in the baths reach fixed values, valves are opened to stream water into two jackets. The temperature difference is imposed almost suddenly. The sidewall temperatures are adjusted until they reach the desired constant values. Then, experiments are conducted. Sufficient time, typically longer than two hours, was allowed for establishing constant wall temperatures before a run after the baths were heated. Subsequent runs at other temperatures could be conducted after about one hour.

2.2. *Unsteadiness of the cell*

The experimental results in this subsection are given for an aspect ratio $A = 15$ ($W = 20$ mm) and a Prandtl number $Pr = 125$.

We made simultaneous measurements of fluid temperatures and flow patterns. Figure 2 shows typical temperature fluctuations and photographs of flow patterns taken at three different times for $Ra = 1.80 \times 10^6$. The measurements were made at the midpoint ($x^*/W = 0.5$, $z^*/H = 0.5$) two and a half hours after the start of the experiment. The hot wall is on the left side in every photograph and the line by the left photograph indicates the midheight of the slot. This Ra corresponds to the critical value at which tertiary cells begin to appear, and the critical value for the onset of secondary cells was $Ra = 5.5 \times 10^5$ (Wakitani 1994). In every photograph, some small tertiary cells can be seen between secondary ones around the core region of the slot.

The measured temperature shows steplike and distinctive variations at unequal time intervals of about 12 to 20 min with slow variations. The time intervals are somewhat larger than the turnover time of a primary cell, typically a few minutes for this Ra. From simultaneous measurements of temperatures at various horizontal positions on the midplane, we confirmed that the temperature was nearly two-dimensional except near the top and bottom. After the distinctive variations, small oscillations appear in the temperature. The temperature plots demonstrate that secondary or tertiary cells are unsteady at this Ra.

The photographs show that two secondary cells in the central portion of the slot have merged with the passage of time. The middle photograph reveals that the steplike and distinctive variation in temperature around there is attributable to the merging of the two secondary cells. A thermocouple is in the lower of two secondary cells which merge, as seen from the left photograph. The temperature increases with height but is nearly constant inside a secondary cell (Lee & Korpela 1983; Wakitani 1994). The temperature in the upper cell is higher than the lower one. When the merging occurs, their temperatures are averaged and the output of the thermocouple increases. The slow fluctuation in temperature among the distinctive variations is due to the moving of a cell. Though it was difficult to detect the unsteady temperature near the critical condition for the onset of secondary cells, we could confirm from visual inspection that a weak unsteadiness of secondary cells appears around a Rayleigh number slightly higher than the critical one.

Figure 3 shows successive photographs of flow patterns taken at intervals of 30 s for $Ra = 9.4 \times 10^5$ three and a half hours after the start of the experiment. At first (figure 3*a*) we can see six secondary cells in the slot. Then one of the middle secondary cells draws in the upper or lower one (figure 3*e* or 3*b*) and the secondary cells merge (figure 3*f* or 3*c*). Before or after the merging, a new secondary cell begins to appear from outside the region filled by the secondary cells, though its appearance is not so clear as the merging. The number of secondary cells changes in the range from four to six. A similar process was observed in the unsteady multicellular flow

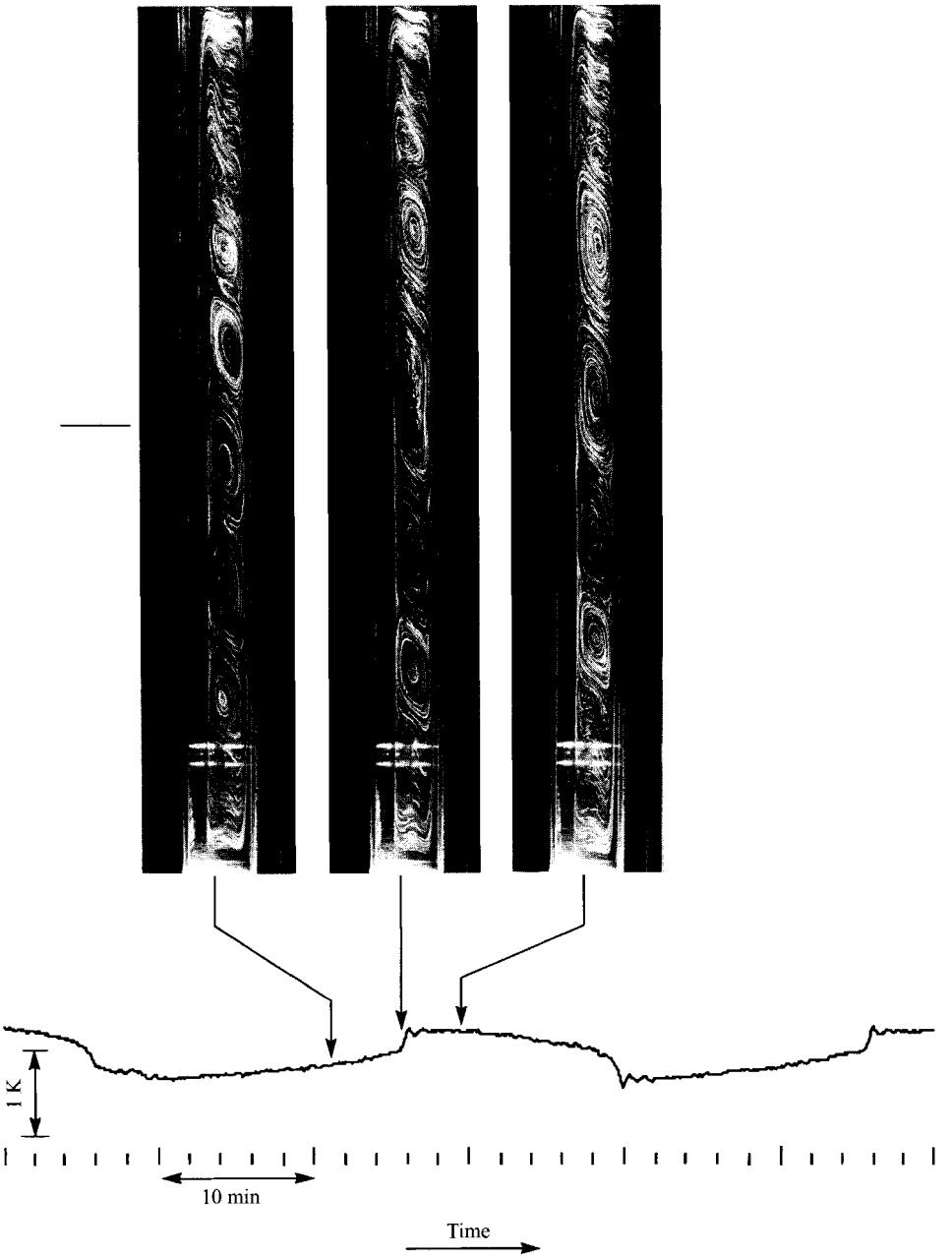

FIGURE 2. Measured temperature and photographs of flow patterns for $Pr = 125$, $A = 15$ and $Ra = 1.80 \times 10^6$. The hot sidewall is to the left in each photograph. The line by the left photograph indicates the midheight of the slot and the arrow indicates the time at which each photograph was taken.

formed by two or three secondary cells for other aspect ratios ($A = 10$ and 20), and $Pr = 900$. The merging and appearance of secondary cells for $Pr = 900$ occurred with longer periods than for $Pr = 125$. The difference in timescales between their periods seems to be roughly consistent with the scaling $Pr^{1/2}$ at the same Ra. The splitting of secondary cells was not observed. To our knowledge, no numerical approach

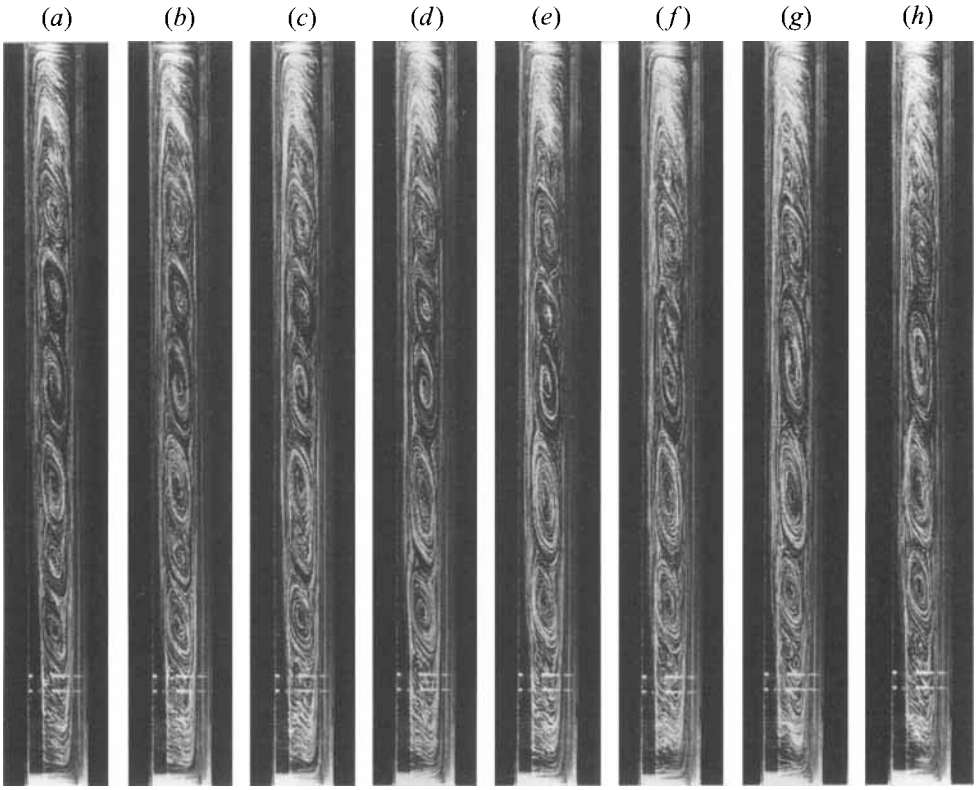

FIGURE 3. Successive photographs of flow patterns for $Pr = 125$, $A = 15$ and $Ra = 9.4 \times 10^5$. Photographs (*a*) to (*h*) were taken at time intervals of 30 s.

has yet simulated this experimental result. The merging and appearance of cells are considered characteristic for large Prandtl number fluids.

3. Numerical simulations

3.1. *Governing equations*

We consider two-dimensional natural convection of a Newtonian fluid in a vertical slot of height H and width W as shown in figure 1. The left and right sidewalls are held at constant temperatures T_1 and T_2, respectively. The top and bottom of the slot are thermally insulated. We assume that the fluid satisfies the Boussinesq approximation but its dynamic viscosity μ^* is a function of temperature T^*. According to Ostrach's suggestion (1988) for natural convection for $(Ra/Pr)^{1/2} \geqslant 1$ and $Pr > 1$, we introduce $V_r = (g\beta\Delta T W\kappa/\nu)^{1/2}$ as reference velocity.

The equations that govern the velocity, pressure and temperature fields are the continuity equation, Navier–Stokes equations and energy equation. These equations can be put into non-dimensional forms by scaling length with the width W, velocity with V_r, pressure with ρV_r^2, temperature with ΔT and time with $W/V_r = (Pr/Ra^{1/2})W^2/\nu$, where ρ is density. The dimensionless temperature is defined as $T = (T^* - T_r)/\Delta T$ with $T_r = (T_1 + T_2)/2$.

We consider the effect of temperature-dependent viscosity on the flow. Therefore, using an exponential approximation, we take the dimensionless viscosity as $\mu = \mu^*/\mu_r = \exp[-a(T^* - T_r)] = \exp(-cT)$, where c is positive for common fluids. The kinematic viscosity ν in (1.1) and (1.2) is μ_r/ρ. This viscosity-temperature relation

with a constant c is a good approximation for fluid such as transformer oil or aqueous glycerol solution. The governing equations can be written in the following non-dimensional forms:

$$\frac{\partial u}{\partial x}+\frac{\partial w}{\partial z}=0, \tag{3.1}$$

$$\frac{\partial u}{\partial t}+u\frac{\partial u}{\partial x}+w\frac{\partial u}{\partial z}=-\frac{\partial p}{\partial x}+\frac{Pr}{Ra^{1/2}}\left\{\frac{\partial}{\partial x}\left(2\mu\frac{\partial u}{\partial x}\right)+\frac{\partial}{\partial z}\left[\mu\left(\frac{\partial u}{\partial z}+\frac{\partial w}{\partial x}\right)\right]\right\}, \tag{3.2}$$

$$\frac{\partial w}{\partial t}+u\frac{\partial w}{\partial x}+w\frac{\partial w}{\partial z}=-\frac{\partial p}{\partial z}+Pr\,T+\frac{Pr}{Ra^{1/2}}\left\{\frac{\partial}{\partial x}\left[\mu\left(\frac{\partial w}{\partial x}+\frac{\partial u}{\partial z}\right)\right]+\frac{\partial}{\partial z}\left(2\mu\frac{\partial w}{\partial z}\right)\right\}, \tag{3.3}$$

$$\frac{\partial T}{\partial t}+u\frac{\partial T}{\partial x}+w\frac{\partial T}{\partial z}=\frac{1}{Ra^{1/2}}\nabla^2 T, \tag{3.4}$$

where t is the time, u and w are the velocity components in the x- and z-directions respectively, p the deviation from the hydrostatic pressure and ∇^2 the Laplacian operator.

The boundary conditions are

$$u=w=0 \quad \text{on} \quad x=0,\ 1;\ z=0,\ A, \tag{3.5}$$

$$T=0.5 \quad \text{on} \quad x=0 \quad \text{and} \quad T=-0.5 \quad \text{on} \quad x=1, \tag{3.6}$$

$$\frac{\partial T}{\partial z}=0 \quad \text{on} \quad z=0,\ A. \tag{3.7}$$

As the initial condition, a motionless state and uniform temperature are taken:

$$u=w=T=p=0 \quad (0<x<1,\ 0<z<A) \quad \text{at} \quad t=0, \tag{3.8}$$

unless otherwise described.

3.2. *Numerical algorithm*

The numerical technique used in the present study is based on the finite difference method of Kawamura & Kuwahara (1984). First, the Poisson equation for the pressure, which is derived from (3.2) and (3.3), is solved, subject to the appropriate boundary conditions. The equation of continuity (3.1) is satisfied at each time step. Then, the velocity and temperature at the next time step are computed from discretized ones of (3.2)–(3.4) using the Euler implicit scheme. The nonlinear terms in (3.2)–(3.4) are linearized and approximated by means of a third-order upwind scheme (Kawamura & Kuwahara 1984; Kawamura, Takami & Kuwahara 1986). The spatial derivatives in the remaining terms are expressed in terms of second-order central differences. These finite difference equations are solved by using the SOR method.

An orthogonal, non-uniform and non-staggered grid system is used. The effects of the grid size and the time increment on the flow characteristics have been examined, and grids with 25×101 or 31×121 points and the time increment of $\Delta t=0.0005$, 0.001 or 0.002 were chosen for the present computations. The finest grid size near the walls is about three times smaller than the size of the uniform grid. All computations are performed on a workstation (Sun SPARCstation 20 SX8 M502).

3.3. *Unsteady multicellular flow and the effect of variable viscosity*

The numerical simulations presented in this section are performed for an aspect ratio $A=15$. Motionless and uniform-temperature states are usually used as initial conditions for the simulations.

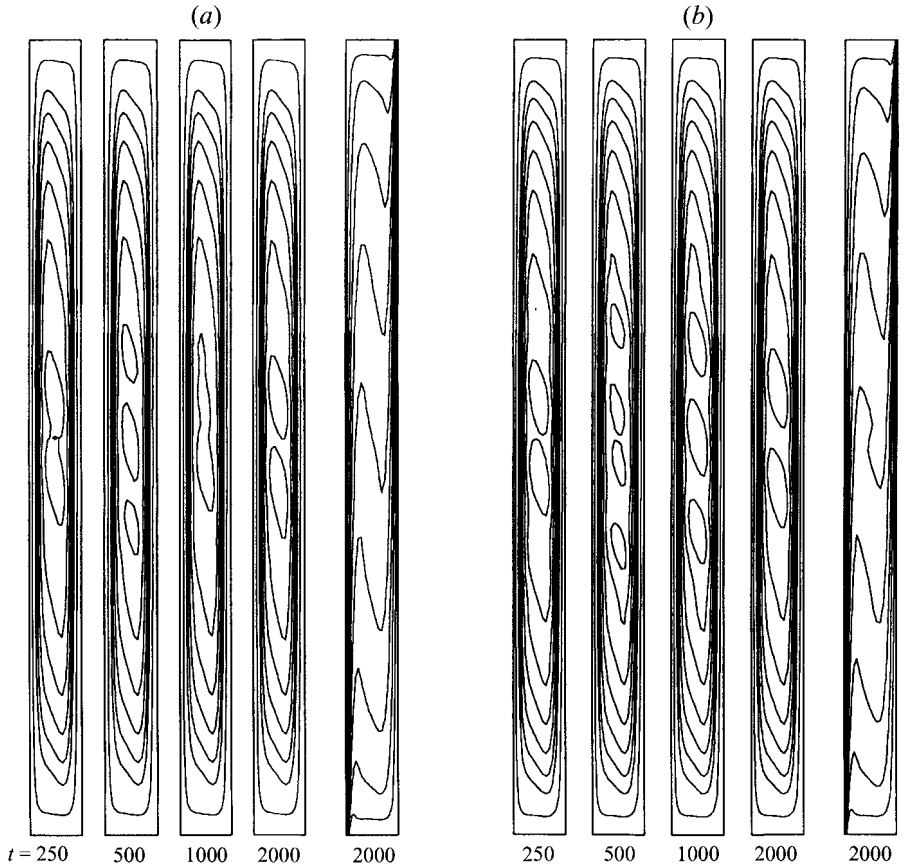

FIGURE 4. Streamlines at four different dimensionless times and isotherms at time $t = 2000$ for constant-viscosity fluids ($c = 0$), $A = 15$, $Ra = 4 \times 10^5$: (*a*) $Pr = 125$; (*b*) $Pr = 1000$. Constant values of the stream function are $-0.05, -0.10, -0.12, -0.14, -0.16, -0.18, -0.20, -0.22$.

Figure 4 shows the streamlines for a constant-viscosity fluid ($c = 0$, $Ra = 4 \times 10^5$) at four different dimensionless times t and the corresponding isotherms at $t = 2000$. The hot wall is on the left side in every figure. This Ra value is slightly higher than the critical Rayleigh number Ra_c at which secondary cells first appear. Figure 4(*a*) presents the result for a Prandtl number $Pr = 125$, and figure 4(*b*) that for $Pr = 1000$. In the case $c = 0$, the critical values are obtained as $Ra_c = 3.82 \times 10^5$ and 3.55×10^5 for $Pr = 125$ and 1000, respectively. We tried several simulations by starting from steady unicellular solutions for $Ra = 3 \times 10^5$, but we obtained the same critical values as those obtained by starting from a motionless state. The critical Rayleigh number for $Pr = 125$ is smaller than that obtained from experiment (Wakitani 1994), in which the flow is not strictly two-dimensional and c has a non-zero value. However, this may be due to secondary cells so weak that their existence cannot be detected from visual observations. The figure demonstrates that the number of secondary cells changes with time even at this Rayleigh number slightly higher than the critical values. Thus the secondary flow is not in a steady state at this Rayleigh number. These simulated results may support the theoretical conclusion of Chait & Korpela (1989) that the secondary flow was periodic in time for $Pr = 1000$.

Figure 5 shows the vertical components of velocities, w-velocities, at the midheight ($z = 7.5$). Figure 5(*a*) shows the w-velocities for a constant-viscosity fluid ($c = 0$) at a

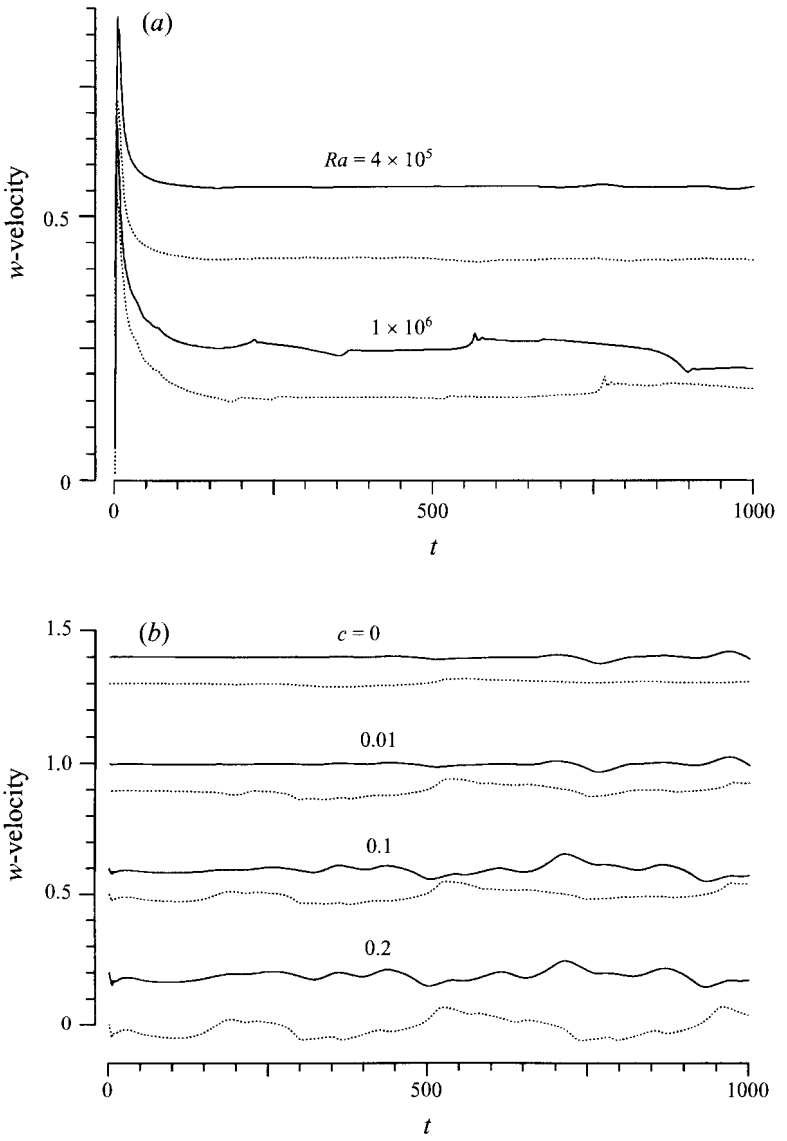

FIGURE 5. Vertical components of velocities simulated for (*a*) a constant-viscosity fluid ($c = 0$) at a point near the hot sidewall at the midheight ($x = 0.053$, $z = 7.5$), and (*b*) variable-viscosity fluids, including the case $c = 0$, for $Ra = 4 \times 10^5$ at the midpoint ($x = 0.5$, $z = 7.5$). $A = 15$; $Pr = 125$ (solid line), $Pr = 1000$ (dotted line). Each line is shifted appropriately in the vertical direction.

point near the hot sidewall ($x = 0.053$), and figure 5(*b*) those for a constant-viscosity fluid and variable-viscosity fluids ($c = 0.01, 0.1, 0.2$) for $Ra = 4 \times 10^5$ at the midpoint ($x = 0.5$). For $Ra = 4 \times 10^5$ in figure 5(*a*), steady state seems to be reached in a dimensionless time $t = 200$, but small variations appear around times larger than $t = 500$. For $Ra = 1 \times 10^6$, on the other hand, apparent variations appear around $t = 200$. Thus, a numerical simulation long enough in time is required to reach an unsteady solution.

As the coefficient of viscosity c is increased, i.e. the temperature-dependency of viscosity becomes strong, unsteady variations begin to occur at a shorter time than for the case $c = 0$ (figure 5*b*). For some values of c, starting from some unicellular

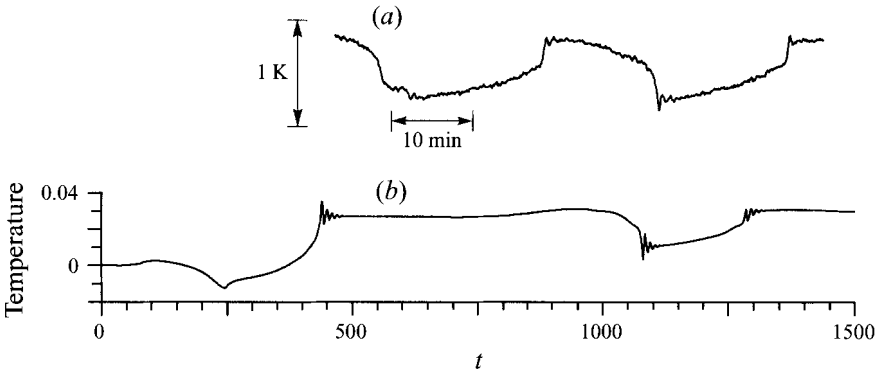

FIGURE 6. Comparison of (*a*) measured temperature and (*b*) simulated temperature at the midpoint ($x = 0.5$, $z = 7.5$) for $c = 0.34$, $Pr = 125$, $A = 15$ and $Ra = 1.8 \times 10^6$. Temperature and timescale are fitted in (*a*) and (*b*).

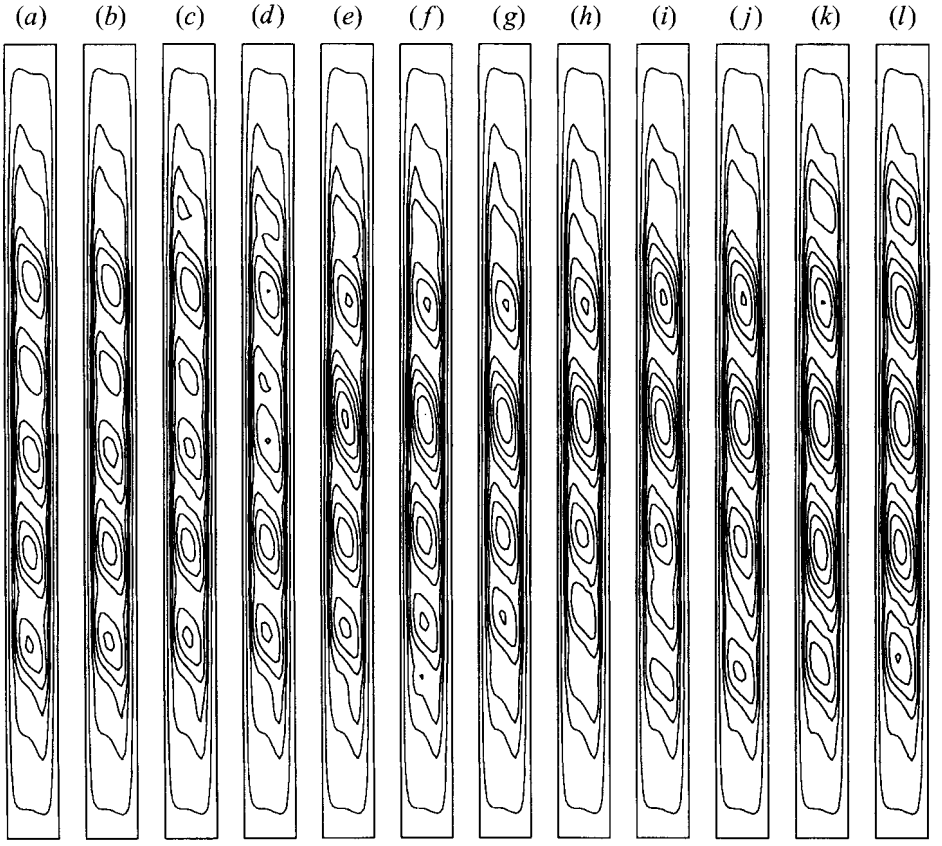

FIGURE 7. Time evolution of streamlines at dimensionless times $t = 1000$ (*a*) to 1132 (*l*) at time intervals of 12 for $c = 0.18$, $Pr = 125$ and $Ra = 9.4 \times 10^5$. Constant values of the stream function are $-0.05, -0.10, -0.12, -0.14, -0.16, -0.18, -0.20, -0.22, -0.24$.

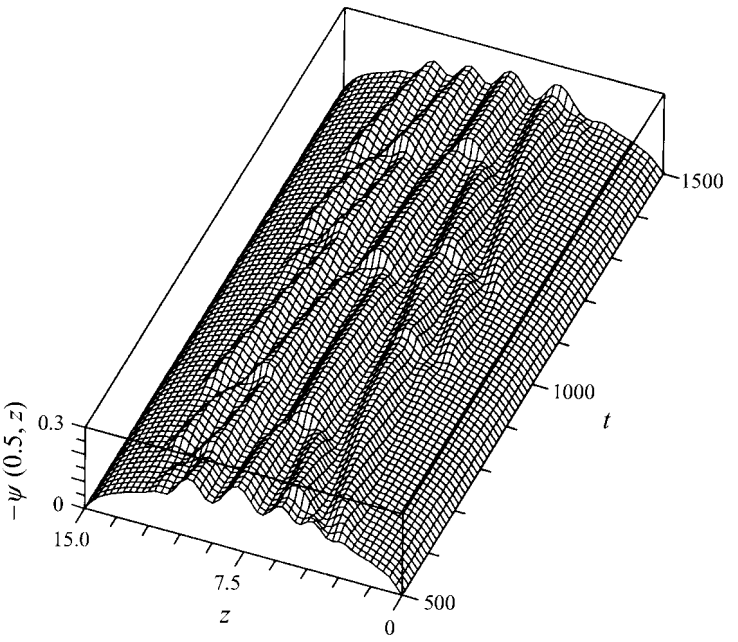

FIGURE 8. Time evolution of the stream function on the midline ($x = 0.5$) for $c = 0.18$, $Pr = 125$, $A = 15$ and $Ra = 9.4 \times 10^5$.

or multicellular solutions, we tried to determine the critical Rayleigh numbers at which secondary cells first appear. These results agree with those obtained from an impulsive run, or starting from a motionless state. As c is increased, however, the onset of instability occurs at a slightly lower Rayleigh number. This trend agrees with the analytical result by Chen & Pearlstein (1989) for an infinite aspect ratio.

Figure 6 shows a comparison of the simulated and measured temperature (the same as shown in figure 2) at the midpoint ($x = 0.5$, $z = 7.5$) for $Ra = 1.8 \times 10^6$. The numerical result is obtained for $c = 0.34$ which agrees with the experimental condition. The simulated result roughly reproduces the experimental one, although the time intervals at which secondary cells merge are different.

Figure 7 shows the time evolution of streamlines for $Pr = 125$ and $Ra = 9.4 \times 10^5$. The figure starts from $t = 1000$ (figure 7*a*) at dimensionless time intervals of 12. This interval corresponds to a time of about 30 s in the present experiment. The value of c is chosen to agree with the experimental condition in figure 3. Two adjacent secondary cells merge successively in such a way that the middle cell draws in the upper or lower one (figure 7*c–e* or 7*h–k*). In this figure, merging takes place three times, though the merging around the upper portion of the slot is not clear. Before or after their merging a new secondary cell originates at the top or bottom of the slot (figure 7*k* or 7*i*). This simulated result reproduces the experimental result in figure 3, qualitatively.

A clearer picture of unsteady secondary cells that merge and appear is obtained from plots of the stream function on the midline $x = 0.5$ as shown in figure 8. Here a peak in the stream function corresponds to the core of a secondary cell and the number of peaks to the number of secondary cells. Figure 8 reveals that as time passes the core of every secondary cell shifts toward the middle of the slot and splitting of secondary cells does not occur.

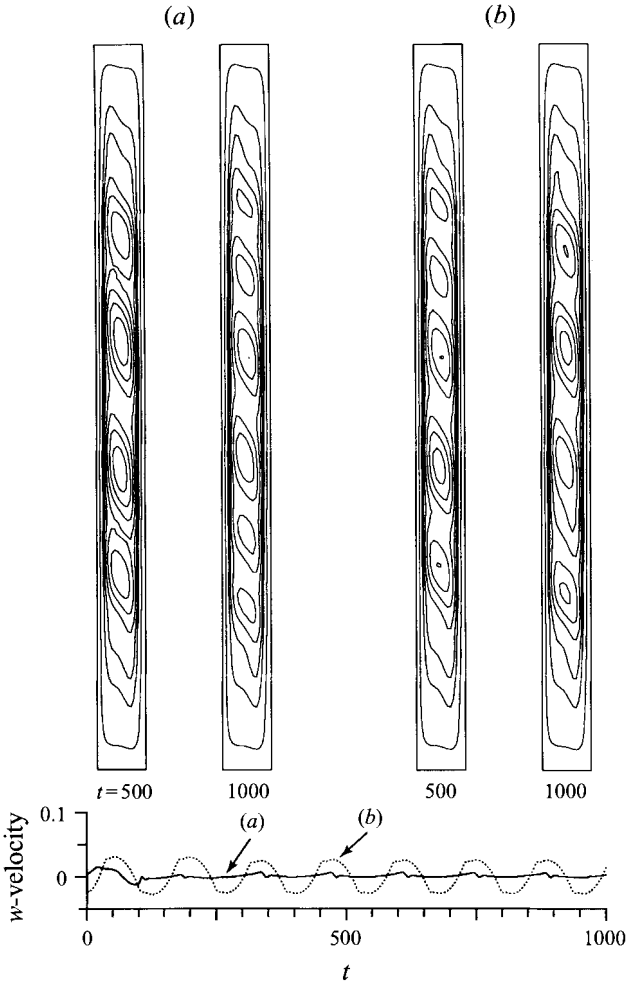

FIGURE 9. Streamlines at dimensionless times $t = 500$, 1000, and vertical components of velocities at the midpoint ($x = 0.5$, $z = 7.5$) for $c = 0$, $A = 15$, $Pr = 125$ and $Ra = 7 \times 10^5$. Results are obtained by (*a*) starting from a motionless state (impulsive run) and (*b*) gradually increasing Ra (gradual run). Constant values of the stream function are $-0.05, -0.10, -0.12, -0.14, -0.16, -0.18, -0.20, -0.22$.

3.4. *Bifurcation phenomena*

To find the dependence of multicellular flow on the initial condition, the numerical calculations are conducted for a constant-viscosity fluid ($c = 0$) of $Pr = 125$ in a vertical slot of $A = 15$ by starting from a motionless state (or impulsive run) and by gradually increasing or decreasing Ra (or gradual run). In the gradual run, after an asymptotic solution has been reached, typically above $t = 1000$, the next calculation is continued by slightly varying Ra.

In steady unicellular or multicellular flow for Ra less than 4×10^5, there is no difference between the solutions from each initial condition. At $Ra = 4 \times 10^5$, the flow becomes unsteady. At this Ra, for the gradual run, a weakly oscillatory shift of secondary cells occurs but their number remains two. For the impulsive run, on the other hand, secondary cells successively repeat their merging and appearance, and the number of secondary cells changes from two to three or three to two (two–three-cell

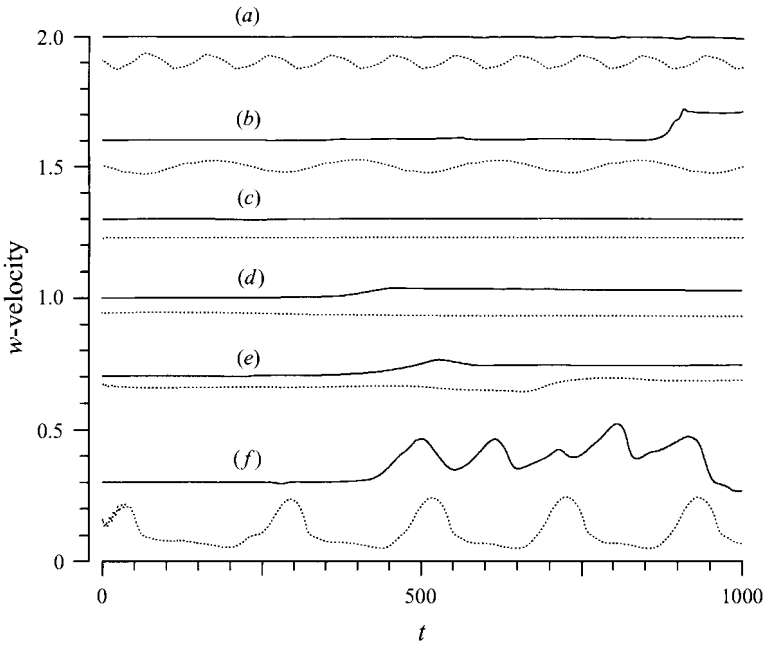

FIGURE 10. Vertical components of velocities at the midpoint ($x = 0.5$, $z = 7.5$) for $c = 0$, $A = 15$ and $Pr = 125$. The solid lines are obtained by starting from a motionless state (impulsive run) and the dotted lines are by gradually increasing Ra (gradual run): (*a*) $Ra = 5 \times 10^5$; (*b*) 1×10^6; (*c*) 4×10^6; (*d*) 1×10^7; (*e*) 2×10^7; (*f*) 4×10^7. Each line is shifted appropriately in the vertical direction.

mode). At $Ra = 4.5 \times 10^5$, a two–four-cell mode appears for the impulsive run and a three–four-cell mode for the gradual run.

As Ra is further increased, each mode translates into a four–six-cell and a four–five-cell mode respectively. At $Ra \approx 9 \times 10^5$, a four–five-cell mode prevails for both runs. Around this Ra tertiary cells begin to appear, but we do not count the weak tertiary cells in the definition of the mode. Figure 9 shows examples of streamlines and vertical velocities at the midpoint for $Ra = 7 \times 10^5$. A distinctive difference in the velocity fluctuations can be seen between the initial conditions. It is considered that our experimental conditions almost correspond to the impulsive run in numerical simulations.

At $Ra \approx 4 \times 10^6$, a three-cell mode with two tertiary cells is established. No shift of the secondary cells can be seen and the flow is almost steady. The quasi-steady state continues to around $Ra = 10^7$. Then the flow becomes unsteady again and the unicellular flow formed by a secondary cell appears (unicell mode). The secondary cell is highly oscillating. This mode is different from the return to the unicellular pattern from the multicellular structure found by Le Quéré (1990) for an air-filled vertical slot.

Figure 10 shows vertical velocities for both runs and figure 11 the streamlines for the gradual run at various Ra. At $Ra = 5 \times 10^5$, the velocity fluctuation for the gradual run is sinusoidal and larger than that for the impulsive run, as shown figure 10(*a*). Figure 10(*c*) demonstrates that the flows are quasi-steady at $Ra = 4 \times 10^6$ for both runs. Figure 11(*b*) shows an example of the flow structure of a three-cell mode in a quasi-steady state. It is again found in the unsteady flow which occurs that the upper and lower of three cells are shifting upwards and downwards respectively (figure 11*d*).

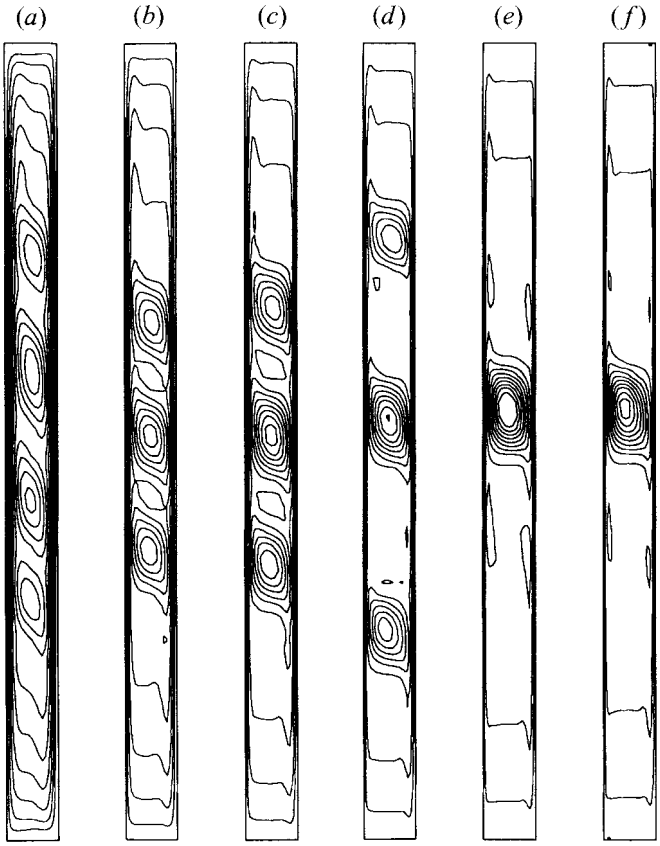

FIGURE 11. Streamlines obtained by gradually increasing Ra (gradual run) at dimensionless times (*a*) $t = 500$ and (*b*)–(*f*) $t = 1000$ for $c = 0$, $A = 15$, $Pr = 125$: (*a*) $Ra = 1 \times 10^6$; (*b*) 5×10^6; (*c*) 1×10^7; (*d*) 2×10^7; (*e*) 4×10^7; (*f*) 5×10^7. Constant values of the stream function are $-0.02, -0.04, -0.06, -0.08, -0.10, -0.12, -0.14, -0.16, -0.18, -0.20, -0.22$.

A flow structure like the one at $Ra = 4 \times 10^7$ in figure 11 (*e*) with small cells along the sidewalls has been observed experimentally by Wakitani (1994) for $A = 10$.

The transition of the cell mode based on the number of secondary cells is summarized in figure 12. The transition from a three-cell mode to a unicell mode at high Ra largely depends on its initial condition. A hysteresis, which is characteristic in bifurcation phenomena, is also found in the transition between a three-cell mode and a unicell mode. However, such a hysteresis cannot be found in the transition between the other modes.

4. Conclusion

In this paper experimental and numerical investigations have been described on natural convection of large Prandtl number fluid in a vertical slot of aspect ratio 15. The numerical results are based on a two-dimensional simulation long enough in time to reach an asymptotic solution for Prandtl numbers of 125 and 1000. The features of the experimental results for a Prandtl number of 125 have been reproduced by the simulation.

The simulation of a constant-viscosity fluid starting from a motionless state needs a long time, typically a dimensionless time larger than 200, until unsteadiness appears in

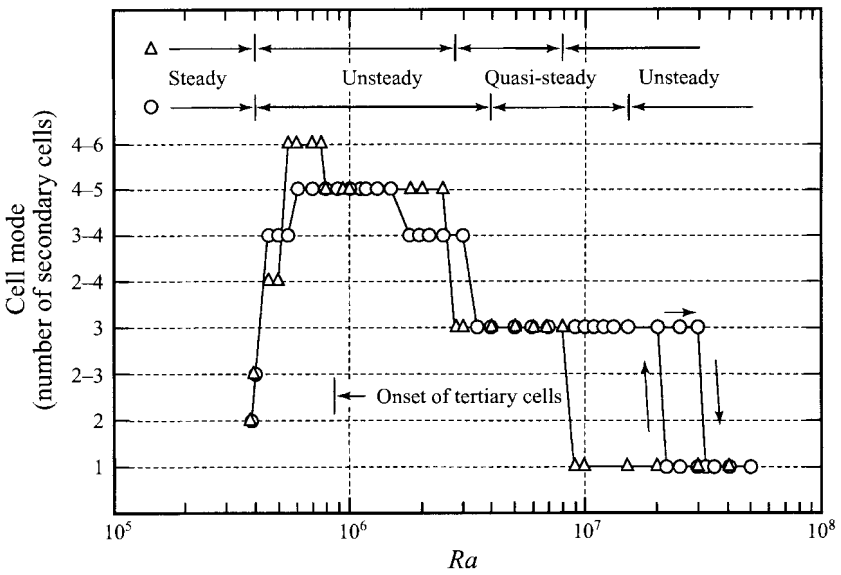

FIGURE 12. Diagram showing the various cell modes for $c = 0$, $A = 15$ and $Pr = 125$. Results are obtained by starting from a motionless state (impulsive run) (△) and by gradually increasing or decreasing Ra (gradual run) (○).

the flow field. On the other hand, as the temperature-dependency of viscosity becomes strong, unsteady variations begin to occur at a shorter time. The unsteady variations are attributed to the moving and merging of secondary cells. The temperature measured in multicellular flow shows steplike and distinctive variations, with long and varying periods, due to the merging of two secondary cells. The secondary flow is in an unsteady state even at a supercritical condition slightly higher than the critical Rayleigh number at which secondary cells appear. The number of secondary cells changes with time.

At the supercritical condition, two adjacent secondary cells merge successively in such a way that a middle cell draws in an upper or lower one. Before or after their merging, a new secondary cell originates from outside the region filled by the secondary cells. This scenario occurs at a Rayleigh number lower than the one at which tertiary cells appear. The merging and appearance are considered characteristic for multicellular flow of a large Prandtl number fluid in a vertical slot.

The computational result demonstrates that the cell mode depends on the initial condition. As the Rayleigh number is increased, the flow becomes unsteady and the number of secondary cells increases. Subsequently, the flow becomes quasi-steady at Rayleigh numbers in some region, in which three secondary cells are formed. Then the flow becomes unsteady again and is a unicellular one formed by a single secondary cell. The simulation does not show the reverse transition from multicellular to unicellular structure found in an air-filled vertical slot. A hysteresis, characteristic in bifurcation phenomena, is found in the transition between the modes at high Rayleigh numbers.

The author gratefully acknowledges the valuable comments of referees on improving the original manuscript. This work is partially supported by Grant-in-Aid for Scientific Research Nos. 61750044 and 62750048 from the Ministry of Education, Science and Culture of Japan.

REFERENCES

BATCHELOR, G. K. 1954 Heat transfer by free convection across a closed cavity between vertical boundaries at different temperatures. *Q. J. Appl. Maths* **12**, 209–233.

BERGHOLZ, R. F. 1978 Instability of steady natural convection in a vertical fluid layer. *J. Fluid Mech.* **84**, 743–768.

CHAIT, A. & KORPELA, S. A. 1989 The secondary flow and its stability for natural convection in a tall vertical enclosure. *J. Fluid Mech.* **200**, 189–216.

CHEN, C. F. & THANGAM, S. 1985 Convective stability of a variable-viscosity fluid in a vertical slot. *J. Fluid Mech.* **161**, 161–173.

CHEN, Y. M. & PEARLSTEIN, A. J. 1989 Stability of free-convection flows of variable viscosity fluids in vertical and inclined slots. *J. Fluid Mech.* **198**, 513–541.

ECKERT, E. R. G. & CARLSON, W. O. 1961 Natural convection in an air layer enclosed between two vertical plates with different temperatures. *Intl J. Heat Mass Transfer* **2**, 106–120.

ELDER, J. W. 1965 Laminar free convection in a vertical slot. *J. Fluid Mech.* **23**, 77–98.

KAWAMURA, T. & KUWAHARA, K. 1984 Computations of high Reynolds number flow around a circular cylinder with surface roughness. *AIAA Paper* 84-0340.

KAWAMURA, T., TAKAMI, H. & KUWAHARA, K. 1986 Computation of high Reynolds number flow around a circular cylinder with surface roughness. *Fluid Dyn. Res.* **1**, 145–162.

LAURIAT, G. & DESRAYAUD, G. 1985 Natural convection in air-filled cavities of high aspect ratios: discrepancies between experimental and theoretical results. *ASME Paper* 85-HT-37.

LE QUÉRÉ, P. 1990 A note on multiple and unsteady solutions in two-dimensional convection in a tall cavity. *Trans. ASME* C: *J. Heat Transfer* **112**, 965–974.

LEE, Y. & KORPELA, S. A. 1983 Multicellular natural convection in a vertical slot. *J. Fluid Mech.* **126**, 91–121.

OSTRACH, S. 1988 Natural convection in enclosures. *Trans. ASME* C: *J. Heat Transfer* **110**, 1175–1190.

ROUX, B., GRONDIN, J., BONTOUX, P. & VAHL DAVIS, G. DE 1980 Reverse transition from multicellular to monocellular motion in vertical fluid layer. *Phys. Chem. Hydrodyn.* **3F**, 292–297.

SEKI, N., FUKUSAKO, S. & INABA, H. 1978 Visual observation of natural convective flows in a narrow vertical cavity. *J. Fluid Mech.* **84**, 695–704.

VAHL DAVIS, G. DE & MALLINSON, G. D. 1975 A note on natural convection in a vertical slot. *J. Fluid Mech.* **72**, 87–93.

WAKITANI, S. 1994 Experiments on convective instability of large Prandtl number fluids in a vertical slot. *Trans. ASME* C: *J. Heat Transfer* **116**, 120–126.